Desalination and Water Treatment
www.deswater.com

doi: 10.5004/dwt.2021.27409

230 (2021) 64–79
August

Techno-economic evaluation of multi-stage vacuum membrane distillation (MSVMD)

Waqas Alam, Muhammad Asif*, Muhammad Suleman

Faculty of Mechanical Engineering, GIK Institute of Engineering Sciences and Technology, Topi 23460, Pakistan, Tel. +92-938-281026; email: masif@giki.edu.pk (M. Asif), Tel. +92-340-5056763; email: waqasalam8138@gmail.com (W. Alam), Tel. +92-343-9194005; email: sulemandaud1995@gmail.com (M. Suleman)

Received 29 January 2021; Accepted 10 May 2021

ABSTRACT

Seawater desalination using conventional vacuum membrane distillation is facing a grave problem of high specific heat consumption (SHC). In order to deal with this issue, energy of the saline feed is recovered in multi-stage vacuum membrane distillation (MSVMD). The present study is aimed to analyze the energetics of MSVMD in terms of SHC, gained output ratio (GOR), and specific membrane area (SMA) as a function of process parameters. An attempt was made to determine the optimum number of stages for the maximum permeate productivity. Further, the impact of multi-staging on MSVMD energetics was also analyzed. A drop in cumulative SHC, GOR, and SMA was found with the corresponding rise in feed inlet temperature. Rising saline feed flowrates enhanced the cumulative SHC and GOR, however, it declined the SMA. The economics of MSVMD in terms of levelized cost of water (LCOW) were also investigated. It was observed that the permeate enhancing conditions such as a rising saline feed temperature from 60°C to 100°C depreciates the LCOW by about 57 USD/m^3. Similarly, a decline in the LCOW was noticed with a surge in saline feed flowrate and vacuum pressure. Multi-staging initially dropped the LCOW, but it was found that after a certain number of stages, further addition would cause an upsurge in the LCOW.

Keywords: Desalination; Membrane distillation; MSVMD; Multi-stage VMD; Vacuum membrane distillation

1. Introduction

Around 25% of the world's total inhabitants have insufficient access to fresh water and a forecasting study suggests that 70% of the total world's populace can face fresh water paucity in the next 10 y [1–3]. This problem is more severe in some parched developing countries, where due to lack of facilities and sufficient experience, supply of consumable water to the abundantly populated cities is a major challenge [4,5]. One way to deal with this water paucity issue is to utilize the sea-water, which is abundantly available, via desalination.

About half a century ago, Bodell [6] was the first one to introduce membrane distillation as a process for water desalination employing water vapor evaporation through a porous aqua phobic membrane [7]. Although, Findley [8] published the first-ever research paper based on membrane distillation in 1967, however, this technique did not receive sufficient attention up until the beginning of 1980s. After that, MD was recognized as a cost-effective and innovative technology for the separation of pure drinkable water [9–11] from briny water. Some of the attractive aspects of MD processes include its capability to be integrated with low-grade energy source requiring lower operating conditions, uncomplicated membrane construction, smaller energy expenditure in case of waste heat, almost 100% salt rejection rate on paper and its bright prospective to utilize low-grade energy source [12–14]. Certain

* Corresponding author.

complications are also associated with the membrane distillation technology, which tend to impact its performance negatively, such as, temperature polarization [15,16], concentration polarization, and conductive heat loss through the membrane [17,18].

The four basic configurations of MD technique include sweeping gas membrane distillation (SGMD), air gap membrane distillation (AGMD), direct contact membrane distillation (DCMD), and vacuum membrane distillation (VMD) [19]. The process of VMDinvolves the application of vacuum pressure, which should be smaller as compared to the saturation pressure of water solvent in the hot feed stream, to the permeate side of membrane [20,21]. The major attribute of VMD is its operationality at considerably lower feed stream temperature and smaller hydrostatic pressure [22,23]. Moreover, it has a higher permeate productivity due to better thermal efficiency and consequently, it is extensively utilized for several MD applications [7,24–28]. Despite having so many advantages over other MD mechanisms, it still has one drawback of high specific heat consumption (SHC) which casts a shadow on its effectiveness. This single drawback has limited the extensive commercialization of the VMD [29,30].

Having worked on all four membrane distillation configurations, researchers are looking for a more energy efficient and cost-effective membrane distillation technique. The flux driving potential of a feed stream is lowered after it has passed through the membrane unit, but it has not lost completely. So, in order to deal with the high SHC issue of VMD, researchers put forth an idea of utilizing sensible heat energy in the membrane exiting stream or the latent heat of condensation in the permeate. The membrane exiting feed stream if entered into another membrane unit can drive out permeate flux which obviously will be lower than its predecessor stage. Such a system which comprises multiple stages of membrane units is called multi-stage membrane distillation. Various multistage mechanisms have been developed based on VMD and AGMD. The main objective was to optimize either the thermal efficiency or the cost associated with the system. Ghaffour et al. [31] discussed various prospects of water productivity and energy efficiency enhancement via hybridization of MD technology with traditional processes such as reverse osmosis (RO), mechanical vapor compression, electro-dialysis, multi-effect distillation, and adsorption. It was found that MD diminishes limitations of RO, when treating concentrated feeds. The MED-MD hybrid system was found to have the most positive effect after hybridization. A cascaded DCMD mechanism was developed by Gilron et al. [32], it was then upgraded by [33] in order to enhance its recovery. Lu et al. [34] performed economic optimization on multi-stage AGMD mechanisms. A multi-stage vacuum membrane distillation (MSVMD) system was designed by Shim et al. [35] and a GOR of less than 1 was reported. Multi-stage VMD system similar to multistage flash distillation (MSF) was developed by Summers [36] and reported a GOR of almost 4. The multistage mechanisms reported a much lower SHC as compared to their single-stage parallels [37]. A company named Memsys, founded in 2009, designed a new MD mechanism named vacuum multi-effect membrane distillation (V-MEMD). A GOR of about 4 was reported for these systems [38]. Memsys VMD technology based on flat sheet membrane arrangement was reported to have about 80% lower SHC than its single-stage counter parallel. Similarly, various other researchers reported a drop in the SHC for systems based on memsys technology [39,40]. Module packing density also plays a vital role in the performance of MD systems based on permeate productivity. Despite the improvement in SHC, a lower module packing density associated with flat sheet membrane systems restrains its permeate productivity [41]. Contrary to flat sheet membrane systems, hollow fiber systems have appreciably high module packing density resulting in enhanced permeate productivity [42–45].

The MSVMD being a new concept has received a very limited attention. Fig. 1 is a representation of the number of articles published on single stage VMD against the number of papers published on MSVMD, on yearly basis over a period of 10 y from 2010 to 2020. It indicates that the first research article on MSVMD was published just recently in 2013 and a very limited literature is available on it as of now.

After an extensive analysis of previously published studies on MSVMD, it was found that very few researchers have investigated it energetics as a function of various process variables. Moreover, no attempt was made in the past to investigate the performance based on each stage of an MSVMD setup. To the best of the author's knowledge, the SHC, GOR, and SMA, have never been investigated with the approach to determine the impact of having additional stages in an MSVMD setup. Furthermore, no published work has been found that focused to investigate the economics of MSVMD as a function of number of stages.

The current study is aimed to analyze MSVMD process technically and economically. An integrated heat and mass transfer model was developed for a hollow fiber MSVMD setup to analyze it numerically. The numerical results were verified experimentally. The cumulative energetics of MSVMD in terms of SHC, GOR, and SMA were analyzed based on process variables such as saline feed inlet temperature and flowrate. An effort was made to study the impact of multi-staging in MSVMD on its cumulative SHC, GOR, and SMA. Lastly, the economics of MSVMD were studied in terms of its levelized cost of water (LCOW) and the impact of process variables on it was investigated. Further, the impact of adding stages to an MSVMD setup on its LCOW was also examined.

2. Theory

2.1. Model for heat transfer

In VMD operation, a convection heat transfer occurs from the bulk feed stream to the feed side membrane interface. This convection heat transfer can be mathematically expressed as:

$$Q_f = h_f\left(\pi d_o N_f\right)\left(T_b - T_i\right) \tag{1}$$

where $(T_b - T_i)$ represents the temperature difference between bulk feed and feed side membrane, d_o is the outer fiber diameter, N_f is the number of fibers in the shell and h_f

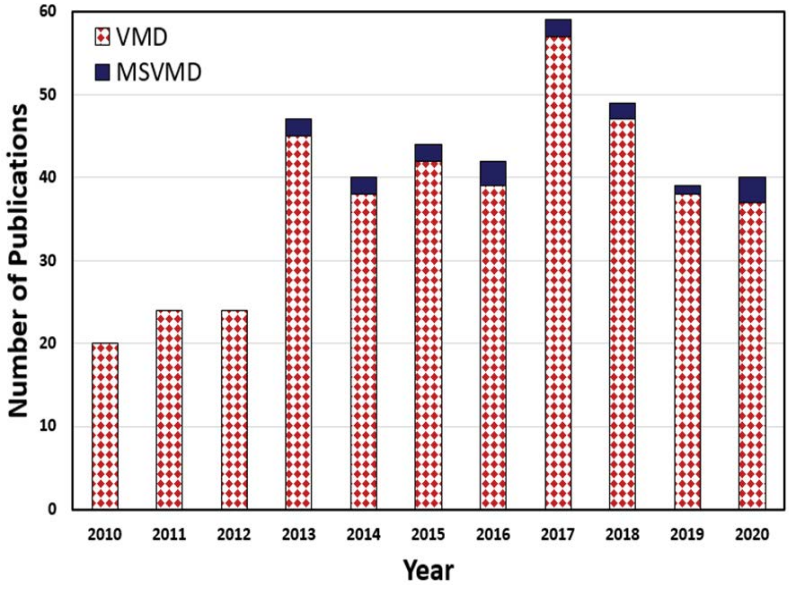

Fig. 1. Research activity on VMD and MSVMD 2010–2020, (Source: Google Scholar).

represents the convective heat transfer coefficient of saline feed.

The convective heat transfer coefficient h_f can be mathematically expressed by Groehen's relation as [46].

$$N_u = \frac{h_f d_h}{k_f} = 0.206\left(\mathrm{Re}\cos\theta\right)^{0.63}\mathrm{Pr}^{0.36} \tag{2}$$

where Re and Pr represent the Renold's number and Prendtl number, respectively, d_h is the shell hydraulic diameter, θ represents the yaw angle, and k_f is the feed thermal conductivity.

Another type of heat transfer associated with the VMD process is heat which is transferred via vapors of permeate through the membrane pores in the form of latent heat. It can be mathematically expressed by the following relation

$$Q_m = Jg_v \tag{3}$$

where g_v and J represent the saturated water enthalpy and permeate flux, respectively.

For high fractional void volume/porosity membranes, the conduction heat loss through the membrane body is negligible. If there is no conduction heat loss considered through the membrane body, the heat loss between bulk feed and feed side membrane interface must be equal to the latent heat transferred via permeate vapors [47].

$$Q_f = Q_m \tag{4}$$

2.2. Model for mass transfer

The mass transfer of vapors across membrane pores either follows Knudsen diffusion model or the Poiseuille flow model, depending upon a dimensionless number called the Knudsen number. The Knudsen number can be mathematically written as

$$k_n = \frac{\lambda}{L} \tag{5}$$

where λ represents the mean free molecular path and L is the characteristic length in which flow through membrane pores is the mean pore size/diameter.

For a non-continuum model, a Knudsen number of less than 1 specifies Poiseuille flow, whereas, a Knudsen number of greater than 1 means that the mass transfer via Knudsen diffusion model is dominant [48]. Mostly in VMD, the mean free molecular path is much greater than the pore sizes of membrane. Hence, the mass transfer across the membrane in VMD is controlled by Knudsen diffusion predominantly. The permeate mass flux in case of Knudsen diffusion model is calculated using the following relation:

$$J_k = 1.064\frac{r\varepsilon}{\tau\delta}\left(\frac{M}{RT_{\mathrm{avg}}}\right)^{0.5}\left(P_i - P_v\right) \tag{6}$$

where $(P_i - P_v)$ represents the vapor pressure drop across the membrane and τ, δ, r and ε are the membrane tortuosity, membrane thickness, mean pore size, and the membrane fractional void volume/porosity, respectively. M, R, and T_{avg} represent the molecular weight of water, universal gas constant, and the absolute temperature in membrane pores, respectively.

3. MSVMD numerical model

In a VMD process, the heat transfer and mass transfer are completed. When the process is at steady-state condition, the total energy and mass balance can be expressed as:

$$Q = h_f\left(T_b - T_i\right) = Jg_v = C_m = 1.064\frac{r\varepsilon}{\tau\delta}\left(\frac{M}{RT_{\mathrm{avg}}}\right)^{0.5}\left(P_i - P_v\right)g_v \tag{7}$$

g_v represents the enthalpy of vaporization of the feed stream and can be calculated using the following correlation [49].

$$g_v = \left(2501.689845 + 1.806916015T_i + 5.087717\right) \times 10^{-4}T_i^2 - \left(1.1221\right)\times 10^{-5}T_i^3 \quad (8)$$

4. Performance indicators

4.1. Specific heat consumption

The total amount of heat energy consumed by the MD setup for a permeate production of 1 m^3 is referred to as its SHC. It can be evaluated using the following equation [50].

$$\text{SHC} = \frac{Q_m \times \rho_f}{\dot{m}_p \times A \times 3{,}600} \quad (9)$$

where ρ_f is the feed inlet solution density, $\dot{m}_p$ is the mass permeate flux in kg/m^{2}s and A represents the total area of membrane in m^2. Q_m is the total heat flux drawn in the form of permeate through the membrane module. It is estimated using the following mathematical relation [51]:

$$Q_m = \dot{m}_f \times c_p \times \left(T_{f,\text{in}} - T_{f,\text{out}}\right) \quad (10)$$

where ($T_{f,\text{in}} - T_{f,\text{out}}$) is the total temperature drop of the hot feed solution between membrane inlet and exit.

4.2. Gained output ratio (GOR)

The ratio of minimum heat energy required to produce the fresh water/permeate, to the total amount of heat input to the system is referred to as gained output ratio. For MD systems, the GOR can be evaluated using the following equation [52]

$$\text{GOR} = \frac{\dot{m}_p \times A \times h_{\text{fg}}}{\dot{Q}_{\text{in}}} \quad (11)$$

where h_{fg} is the enthalpy of vaporization (kJ/kg) at the feed inlet temperature and $\dot{Q}_{\text{in}}$ is the total power input to the system in kW.

4.3. Specific membrane area (SMA)

It is defined as the minimum membrane area required by the system to produce a total permeate output of 1 m^3/d. It can be mathematically expressed in the form of following equation [37]:

$$\text{SMA} = \frac{A}{\dot{V}_{p,\text{total}}} \quad (12)$$

where A (m^2) is the total membrane area of the system and $\dot{V}_{p,\text{total}}$ (m^3/d) is the total volumetric permeate production of the system per day.

5. MSVMD economic model

This economic model for the multistage vacuum membrane distillation (MSVMD) setup takes into consideration all the costs related to the capital equipment, cost along with the installation, maintenance, and operation costs in USD per annum. The equipment capital cost comprises of the following costs in USD:

- Membrane cost per unit area
- Water and vacuum pump cost
- The permeate and feed tank cost
- Piping and control system cost

Peters [53] proposed that the installation cost of a distillation plant can be assumed to be 20% of the total equipment capital cost. Park et al. [54] assumed the maintenance cost to be 10% of the VMD cost plus 2% of the equipment capital cost. The operational cost of MSVMD setup comprises of the fuel/electricity cost, the brine disposal cost and the chemical treatment cost. The cost model used in the current study is derived from different references and publications. Kolhe et al. [55] used a term "levelized cost of water (LCOW)" in order to measure the cost effectiveness of membrane distillation systems. LCOW is the average total cost in USD required to produce 1 m^3 of pure water through distillation. In this study, the model of Koner et al. [55] that employs present worth factor (PWF), is used to estimate the LCOW.

$$i_{\text{real}} = \frac{i - i_{\text{inf}}}{1 + i_{\text{inf}}} \quad (13)$$

$$\text{PWF} = \frac{1}{i_{\text{real}}}\left(1 - \frac{1}{\left(1 + i_{\text{inf}}\right)^n}\right) \quad (14)$$

$$\text{LCOW} = \frac{Z_{\text{eqp}} + Z_{\text{ins}} + \text{PWF}\left(Z_{\text{opt}} + Z_{\text{main}}\right)}{\text{PWF} \times \sum \dot{m}_p} \quad (15)$$

where i_{real} is the real interest rate, i is the interest rate, and i_{inf} is the inflation rate. $\dot{m}_p$ is the permeate output of the MSVMD setup in m^3/y. Z is the capital cost in USD and the subscripts eqp, main, ins, and opt represent the equipment, maintenance, installation, and operational costs, respectively. PWF represents the present worth factor. Table 1 presents all the design parameters used in the economic model.

6. System illustration

6.1. Experimental setup

Fig. 2 is a schematic of the main apparatus used for experimentation in the present study. The setup consisted of a feed loop, a cold-water loop, and a vacuum loop.

6.2. Membrane specifications

The membrane used in this study was made of PTFE material manufactured by guochu technology (Xiamen). Table 2 shows the detailed specifications of membrane unit utilized in the current study, as provided by the manufacturer.

Table 1
Operating parameters used in current study

Operating parameters	Symbol	Value ($)	Reference
Interest rate	I	11.19%	Based on current economic situation in Pakistan
Inflation rate	i_{inf}	8%	Based on current economic situation in Pakistan
Operating years	N	20	[30]
MSVMD setup cost	$Z_{capital}$	21,569	Based on commercial quote
Membrane cost	Z_{mem}	90/m^2	Based on commercial quote
Installation cost	Z_{ins}	20% of total setup cost	[56]
Maintenance cost	Z_{main}	2% of the equipment cost	[30]
Electricity cost	Z_{fuel}	0.055/kWh	Based on electricity rates in Pakistan
Brine disposal cost	Z_{BD}	0.0015/m^3	[30]
Chemical treatment cost	Z_{CTC}	0.0018/m^3	[30]

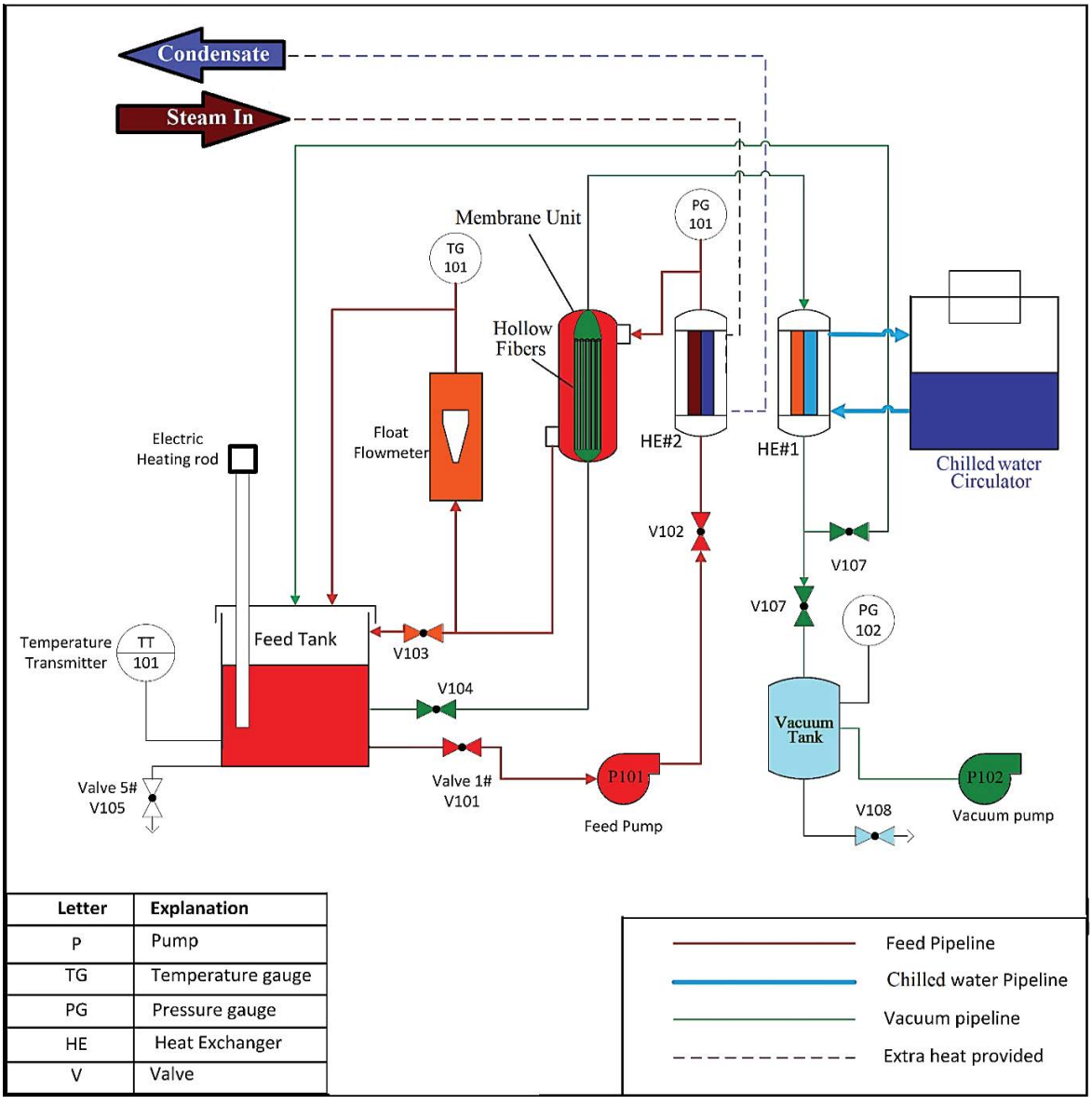

Fig. 2. Layout of experimental setup.

Table 2
Features of membrane unit used in current study

Shell side parameters	Dimensions and features
Shell diameter d_s (mm)	90
Length of the membrane module (mm)	1225
Material	Acrylonitrile butadiene styrene
Fiber parameters	Dimensions and features
Total number of hollow fibers	1,500
Outer diameter of hollow fiber, d_o (mm)	1.6
Inner diameter of hollow fiber, d_i (mm)	0.9
Membrane thickness, δ_m (mm)	0.35
Membrane pore size (μm)	0.5
Membrane porosity	45
Membrane Tortuosity	2
Material	PTFE

For the first stage of each experiment, the required flow rate and temperature of the feed solution were set to the desired value. The system was allowed to reach a steady-state condition denoted by constant reading of temperatures and flow rates. Usually, the time required for the system to achieve the steady-state condition was of the order 25–30 min. 5 min data was recorded for every point in a steady-state condition. The key measurements taken from the experiments were the feed solution temperature value, vacuum pressure value, cooling water temperature, running time, and vacuum tank drainage volume. One of the most vital measurement is the temperature of feed stream as it exits the membrane unit, which is noted from temperature gauge (TG101). For the subsequent stage, a temperature equal to the temperature of exiting feed stream from the previous stage was set and the whole process was repeated while keeping the flowrate constant as in the previous stage. Similarly, all the key measurements were recorded for each subsequent stage. An average of 3 data points was taken for each experiment.

7. Numerical model validation

Experiments were performed to investigate the permeate flux of each individual stage for a 10-stage MSVMD setup at various feed inlet temperatures from 60°C to 70°C and various feed flowrates from 1,000 to 4,000 L/h. The experimental permeate flux data was compared with the numerical results at various feed inlet temperature and feed flow rate as shown in Figs. 3 and 4, respectively. The solid and dashed lines represent the experimental and numerical results, respectively.

In a similar way, the numerically and experimentally determined (SMA)/stage of the setup was compared, by varying feed inlet temperatures from 60°C to 70°C and feed flowrates from 2,000 to 4,000 L/h, as shown in Figs. 5 and 6, respectively.

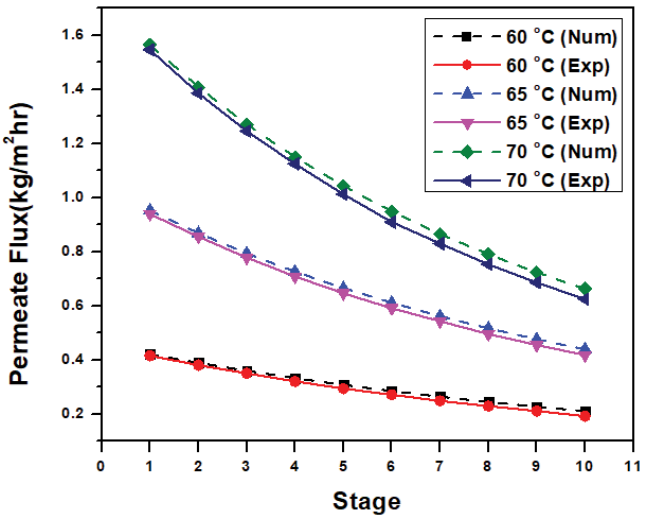

Fig. 3. Numerical and experimental permeate productivity (kg/m² h) of each individual stage for feed temperatures of 60°C, 65°C and 70°C; Dashed lines: Numerical data, Solid lines: Experimental data.

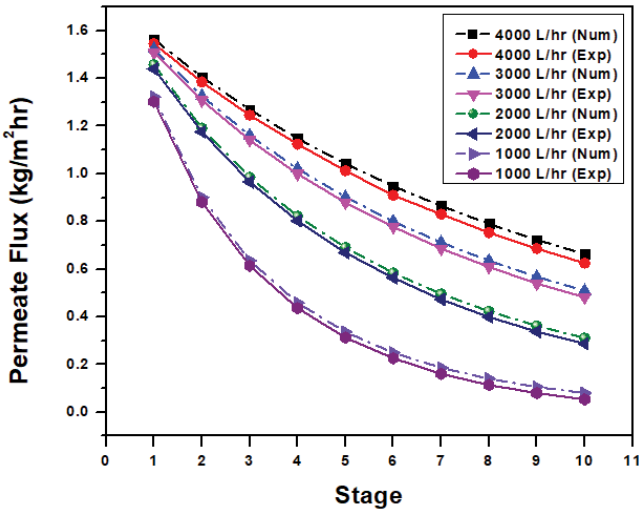

Fig. 4. Numerical and experimental permeate productivity (kg/m² h) of each individual stage for feed flowrates of 1,000, 2,000, 3,000 and 4,000 L/h; Dashed lines: Numerical data, Solid lines: Experimental data.

An average deviation of under 5% can be noted in the above plots. In other words, a good agreement is observed between the numerical and experimental findings.

8. Numerical results and discussion

8.1. Water productivity inversion for process parameters

This section is aimed to investigate the optimum number of stages in MSVMD setup, that ensures the maximum permeate output, and any further addition of stages does not benefit in terms of permeate productivity. In this regard, Fig. 7a and b shows the permeate productivity of

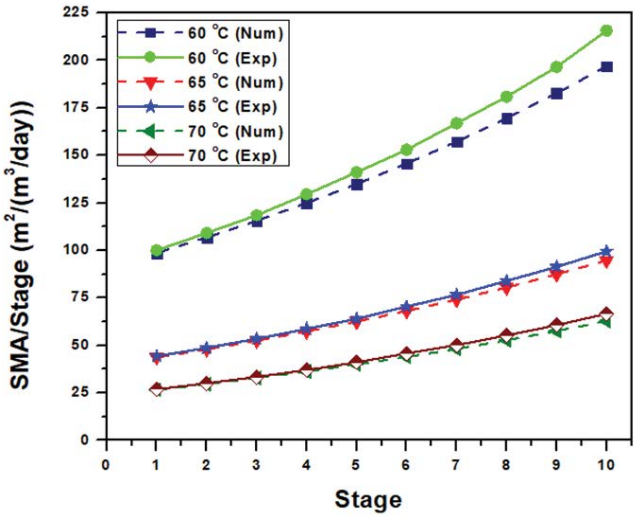

Fig. 5. Numerical and experimental SMA per stage at feed temperatures of 60°C, 65°C and 70°C; Dashed lines: Numerical data, Solid lines: Experimental data.

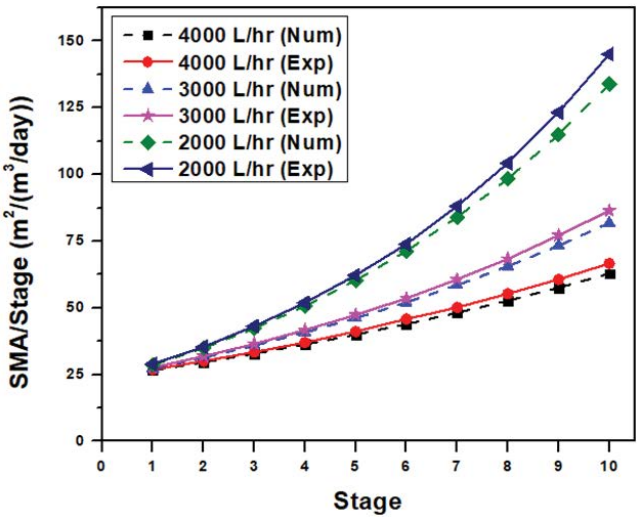

Fig. 6. Numerical and experimental SMA/stage at feed flowrates of 2,000, 3,000 and 4,000 L/h; Dashed lines: Numerical data, Solid lines: Experimental data.

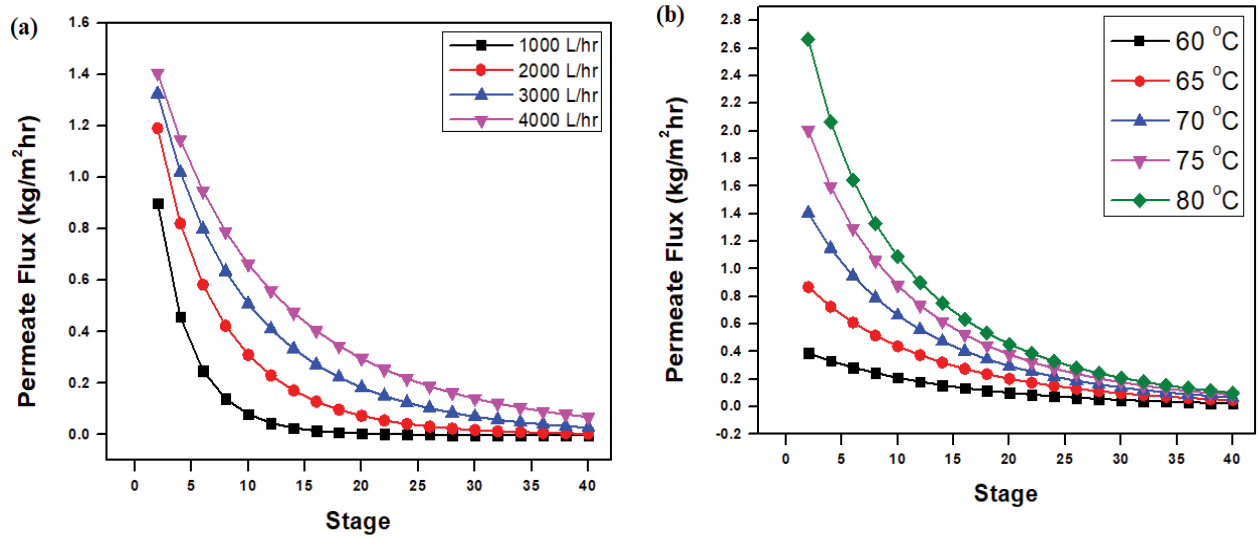

Fig. 7. Individual stage permeate flux at (a) Feed solution flowrate of 1,000, 2,000, 3,000, and 4,000 L/h. (b) Feed solution inlet temperature of 60°C, 65°C, 70°C, 75°C and 80°C.

each individual stage for a 40-stage MSVMD setup, at various feed inlet temperature and flowrate. The results indicated that the individual stage permeate productivity remained high for flux promoting conditions (higher feed temperatures and flowrates), however, beyond a certain number of stages, this behavior reversed and flux promoting conditions yielded a lower individual stage permeate production as compared to flux demoting conditions (lower feed temperatures and flowrates). This point at which this trend reverses is termed as the point of inversion.

8.2. Parametric analysis of MSVMD energetics

This section presents the impact of process parameters on energetic performance of MSVMD in terms of SHC, GOR, and SMA.

8.2.1. Feed inlet temperature

Fig. 8 presents the influence of feed solution inlet temperature on the collective permeate flux of an 18-stage MSVMD setup, over a range of feed flowrates variating from 1,000 to 4,000 L/h. The feed solution inlet temperature was varied from 60°C to 100°C, whereas, the feed concentration was kept constant at 0.31 gm/L.

The results suggest a fall in the collective SHC with the corresponding rise in the feed solution inlet temperature. This behavior can be attributed to the fact that, a permeate surge occurs with the rise in saline feed solution inlet temperature that resulted in decease of SHC, according to Eq. (9). Although, a rise in the feed inlet temperature would also increase the temperature drop ($T_{f,\text{in}} - T_{f,\text{out}}$) across the membrane module, causing the SHC to rise but

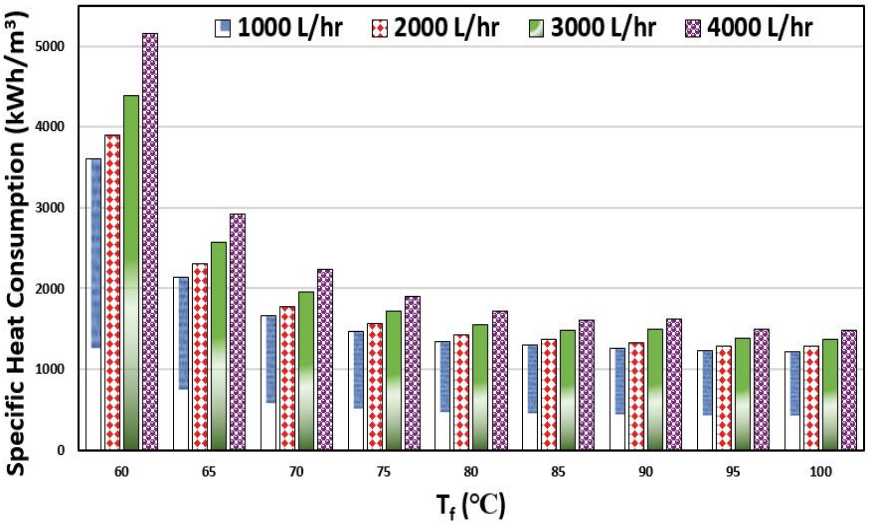

Fig. 8. Impact of saline feed solution inlet temperature on cumulative SHC of MSVMD for feed flowrates ranging from 1,000 to 4,000 L/h.

this increase in temperature drop is trivial compared to the permeate surge it causes along with it.

Furthermore, the plot also suggests that the fall in SHC with the corresponding rise in feed inlet temperature, decreases gradually as the feed inlet temperature continues to raise. This can be due to the fact that at higher temperatures, the temperature drop, ($T_{f,\text{in}} - T_{f,\text{out}}$) across the membrane module is higher, resulting in a small decrease in the SHC with feed temperature.

The impact of saline feed solution inlet temperature on the GOR of an 18-stage MSVMD setup, was investigated over a range of feed flowrates varying from 1,000 to 4,000 L/h and the results depicted in Fig. 9. The feed concentration was kept constant at 0.31 gm/L. The results suggest that an increasing feed inlet temperature causes the GOR to fall irrespective of feed flowrate. The reason behind this behavior is that a higher feed inlet temperature requires a larger total energy input $\dot{Q}_{\text{in}}$ to the system, and GOR being the ratio of minimum heat energy required to the actual energy input to the system ($\dot{Q}_{\text{in}}$), thus falls down. Also, Eq. (11) clearly shows that the total energy input $\dot{Q}_{\text{in}}$ is the denominator term. Although, the feed inlet temperature also raises the collective permeate flux of the system (which is a numerator term in Eq. (11)), this rise in permeate output is negligible as compared to the increase in total energy input it causes.

Fig. 10 presents the impact of feed solution inlet temperature on the SMA of an 18-stage MSVMD setup over a range of feed flowrates, varying from 1,000 to 5,000 L/h. The feed concentration was kept constant at 0.31 gm/L. The plot indicates an inverse relationship between the saline feed solution inlet temperature and the specific membrane area. In other words, a higher feed inlet temperature ensures smaller SMA. This inverse relationship is quite obvious, since it has been established earlier that a higher feed inlet temperature brings about a higher permeate output, eventually leading to a smaller area (m^2) required for a cumulative permeate production of 1 m^3/d.

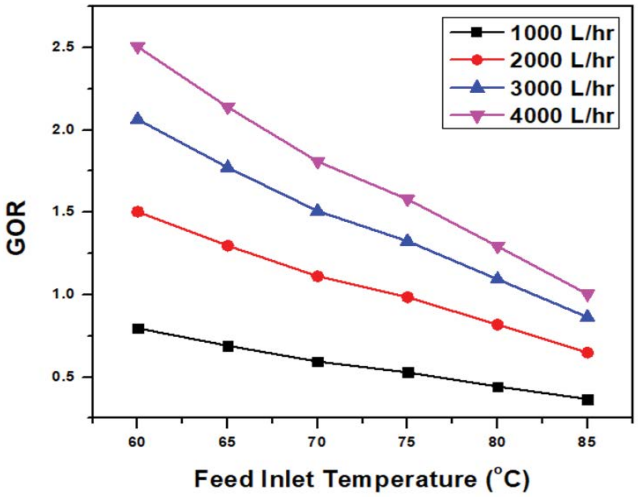

Fig. 9. Impact of feed temperature on cumulative GOR of MSVMD for feed flowrates ranging from 1,000 to 4,000 L/h.

8.2.2. Feed inlet flowrate

Fig. 11 presents a plot for the cumulative SHC of an 18-stage VMD against feed solution flowrate carried out at various feed inlet temperatures from 60°C to 100°C. The feed concentration was kept constant at 0.31 gm/L. The cumulative SHC increased with rise in the feed flowrate, indicating a direct relation between the two. This rising trend of SHC is because the feed mass flowrate ($\dot{m}_f$), being a numerator term in Eq. (10) tends to raise the SHC as the feed flowrate is increased.

Similarly, at higher feed flowrates the temperature drop ($T_{f,\text{in}} - T_{f,\text{out}}$) across the membrane is also higher, which also being a numerator term tends to increase the SHC. Although higher feed flowrates increased the permeate output, yet this increase in permeate output is negligible

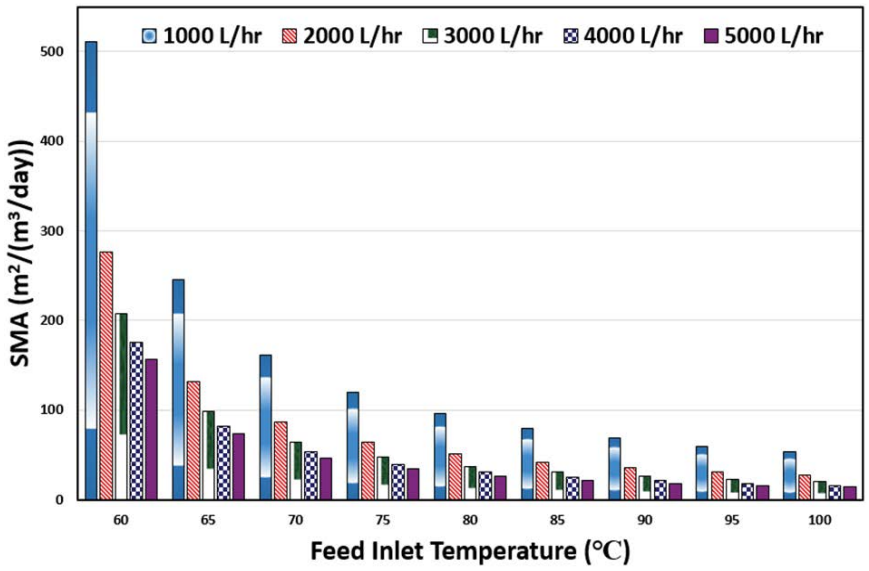

Fig. 10. Impact of feed temperature on cumulative SMA of MSVMD for feed flowrates ranging from 1,000 to 4,000 L/h.

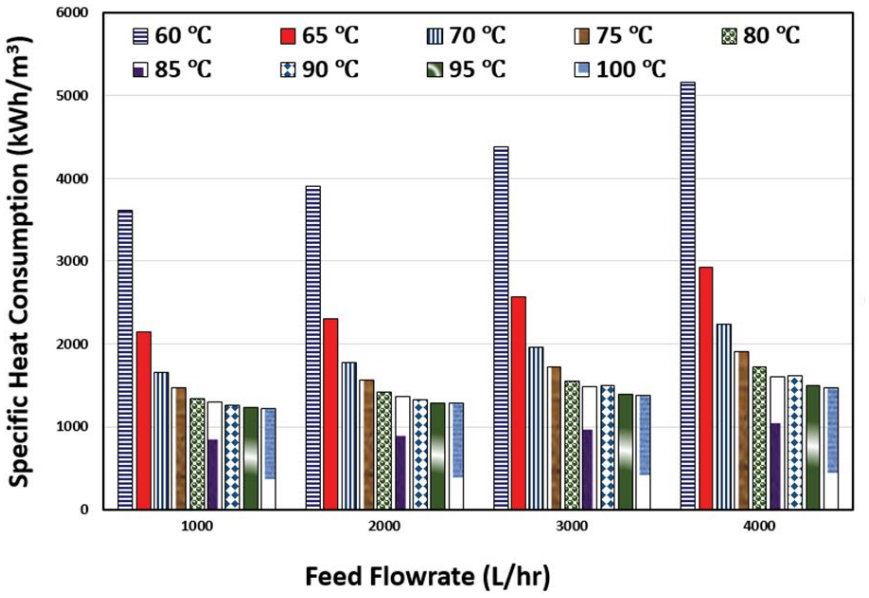

Fig. 11. Impact of feed flowrate on cumulative SHC of MSVMD for feed temperature ranging from 60°C to 100°C.

as compared to the increase in ($\dot{m}_p$) and ($T_{f,\text{in}} - T_{f,\text{out}}$). Hence, the cumulative SHC increases with the increase in feed flowrate.

Fig. 12 exhibits the influence of feed flowrate on the cumulative GOR of an 18-stage MSVMD setup. This investigation was carried out at feed temperature range from 60°C to 80°C , while keeping the feed concentration constant at 0.31 gm/L. The graph specifies a direct relationship between the feed flowrate and the cumulative GOR. This increase in the cumulative GOR can be described by the fact that by increasing the feed flowrate enhances the permeate production of an MSVMD setup, and eventually, the permeate mass flowrate ($\dot{m}_p$) being a numerator term in the relation for the gained output ratio (GOR) (as shown by Eq. (11)) raises the GOR.

Fig. 13 illustrates the influence of feed flowrate on the SMA of an 18-stage MSVMD, over feed inlet temperatures varying from 60°C to 100°C. The concentration was kept constant at 0.31 gm/L. It indicates an inverse relationship between the feed flowrate and the cumulative SMA of an 18-stage MSVMD setup. This decrease in the SMA is evident due to an increase in the permeate output with the flowrate. Moreover, it can be noted that the fall in SMA with the feed flowrate is more evident at lower flowrates whereas it becomes trivial at higher flowrates. For example, for a feed temperature of 60°C, the decrease in cumulative

SMA is 235 $m^2/(m^3/d)$ as the feed flowrate is raised from 1,000 to 2,000 L/h, whereas for a rise in feed inlet flowrate from 4,000 to 5,000 L/h, the decrease in SMA is a meagre 18.35 $m^2/(m^3/d)$.

8.3. Effect of multi-staging on MSVMD energetics

8.3.1. Specific heat consumption

Fig. 14 presents the impact produced on SHC by the addition of stages to the MSVMD setup, over a range of feed inlet temperatures variating from 60°C to 80°C. It is obvious that addition of stages to the MSVMD setup enhances the collective permeate flux, if there is flux driving potential in the brine stream. This increase in the permeate flux with the addition of stages ensures a corresponding decrease in the SHC as can be seen in the plot. For example, at a feed inlet temperature of 60°C, the addition of two stages to a VMD setup, brings down the SHC from 9,288.0139 to 7,645.0225 kWh/m^3.

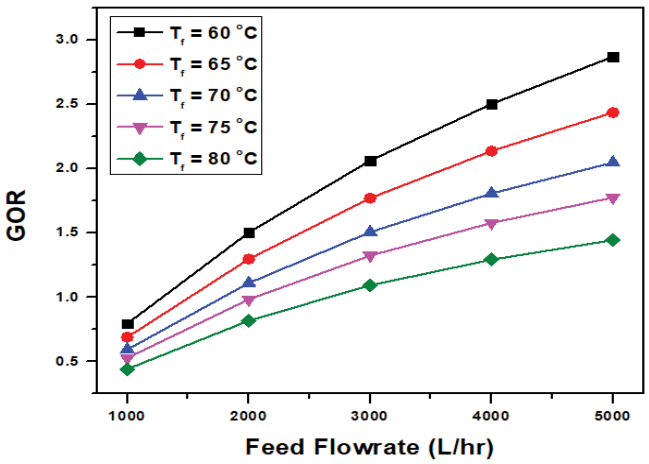

Fig. 12. Impact of feed flowrate on cumulative GOR of MSVMD for feed solution inlet temperature varying from 60°C to 80°C.

8.3.2. Gained output ratio

Fig. 15 presents the impact of multi-staging on GOR of an MSVMD setup, for a range of saline feed solution inlet temperatures variating from 60°C to 80°C. The feed inlet flowrate and concentration were kept constant at 4,000 L/h and 0.31 gm/L, respectively.

The plot indicates that addition of extra stages to an MSVMD setup enhances the GOR if there is flux driving potential in the brine stream. For instance, for a saline feed solution inlet temperature of 60°C, the GOR surges from 0.582 to 2.50 as the number of stages is raised from 2 to 18. This behavior is because addition of stages ensures a higher total permeate output associated with higher membrane area, eventually resulting in a surge in the total GOR for an MSVMD setup.

8.3.3. Specific membrane area

After investigating the effect of additional stages on MSVMD performance in terms of SHC and GOR, it is established that more the number of stages, the better is the performance. This means, an infinite number of stages will give the best performance; however, such a system is far from practical due to the large cost that it would cause. Thus, it is of prime importance to investigate the effect of additional stages in an MSVMD setup on its cost in terms of SMA, and impact on the performance.

Fig. 16 depicts variation in SMA for MSVMD setup having total number of stages varying from 2 to 18, over a range of feed inlet temperatures from 60°C to 80°C. The feed flowrate and concentration were kept constant at 4,000 L/h and 0.31 gm/L, respectively.

An assessment of the plot suggests a direct relation between the number of stages and the SMA. In other words, for a higher number of stages, a higher membrane area is required to produce a cumulative permeate output of 1 m^3/d. The plot shows that, for a feed solution temperature of 60°C, the SMA was increased from 102.60 to 175 $m^2/(m^3/d)$ as the number of stages was increased from 2 to 18 in the MSVMD setup. This behavior is obvious due to the reason

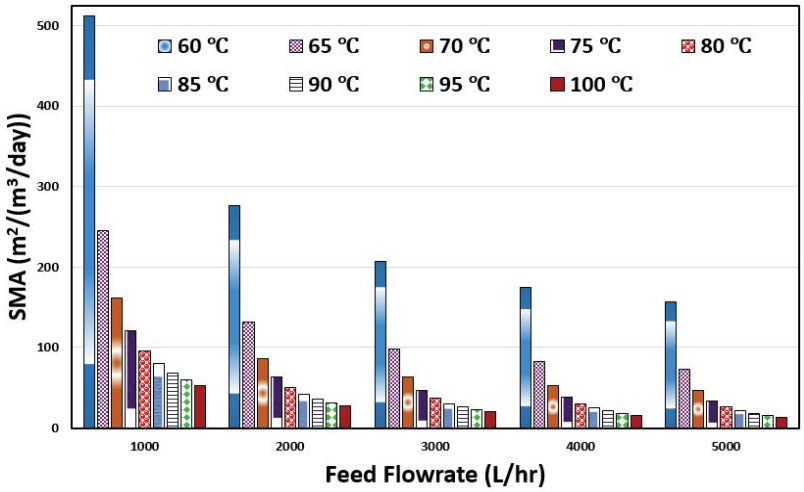

Fig. 13. Impact of feed flowrate on cumulative SMA of MSVMD for feed temperature ranging from 60°C to 100°C.

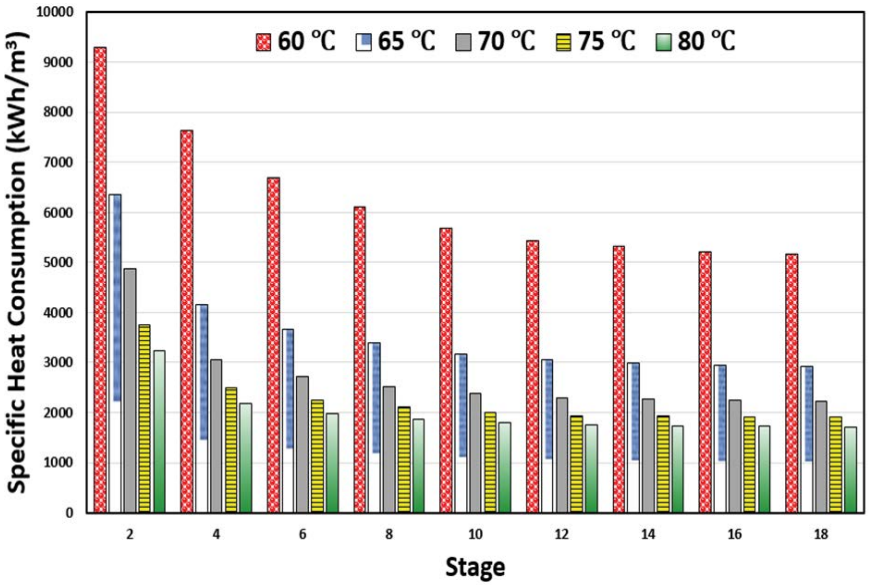

Fig. 14. Effect produced by installation of additional stages on cumulative SHC.

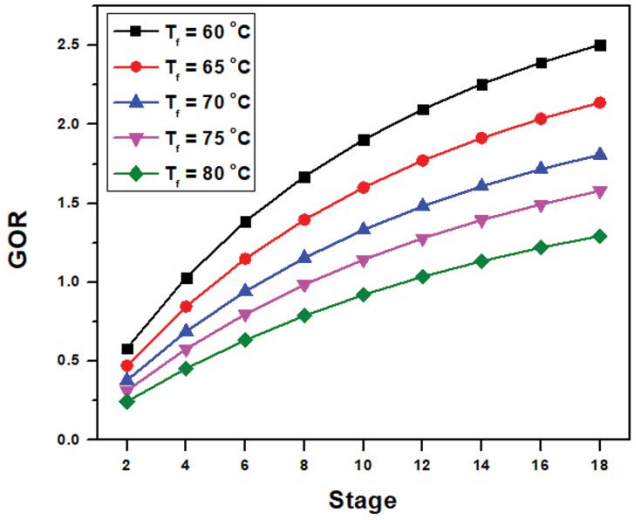

Fig. 15. Effect produced by installation of additional stages on cumulative GOR.

that every successive stage has a lower individual permeate flux as compared to its predecessor. This eventually causes the SMA to rise as the number of stages in an MSVMD setup are enhanced.

8.4. Parametric analysis of MSVMD economics

The impact of various process parameters on the levelized cost of water (LCOW) was investigated and the results are compiled in the form of plots as described below.

8.4.1. Feed solution inlet temperature

Fig. 17 presents the influence of saline feed inlet temperature on the LCOW of MSVMD setup for various feed inlet temperature from 60°C to 100°C, while keeping the feed concentration constant at a value of 0.31 gm/L. The feed flowrate was varied from 1,000 to 4,000 L/h. The results imply that, at higher feed temperatures a less cost is required to produce a permeate output of 1 m^3. For instance, for a feed flowrate of 1,000 L/h, the LCOW drops from 63.4 USD/m^3 at a feed inlet temperature of 60°C to 7.646 USD/m^3 at a feed inlet temperature of 100°C. This ebbtide in LCOW with the feed inlet temperature can be attributed to the fact that rising feed inlet temperature brings about an upsurge in the cumulative permeate production of an MSVMD setup, which ultimately ends up decreasing the LCOW. Although, at higher feed flowrates, the operational cost of the setup also rises in the form of electrical energy consumption, but this increase is trivial compared to the rise in the permeate output.

8.4.2. Feed inlet flowrate

Fig. 18 presents the impact produced on cumulative LCOW of an 18-stage MSVMD, as the feed solution inlet flowrate is varied from 1,000 to 7,000 L/h. This investigation was carried out for various feed solution inlet temperatures from 60°C to 80°C, while keeping the feed concentration and vacuum pressure constant at 0.31 gm/L and 16 kPa, respectively.

The results indicated that an increase in feed flowrate has a positive effect on the LCOW of an MSVMD setup. In other words, the LCOW ebbtides with a rise in the feed inlet flowrate. It can be seen from the graph that the LCOW falls from 63.40 USD/m^3 at a feed temperature and flowrate of 60°C and 1,000 L/h respectively, to 16.92 USD/m^3 at the same feed temperature and a flowrate of 7,000 L/h. The total drop in the LCOW is 46.48 USD/m^3. This soaring trend in the LCOW with the increased feed flowrate is evident due to the increase in the cumulative permeate production of an MSVMD setup. The permeate output ($\dot{m}_p$)

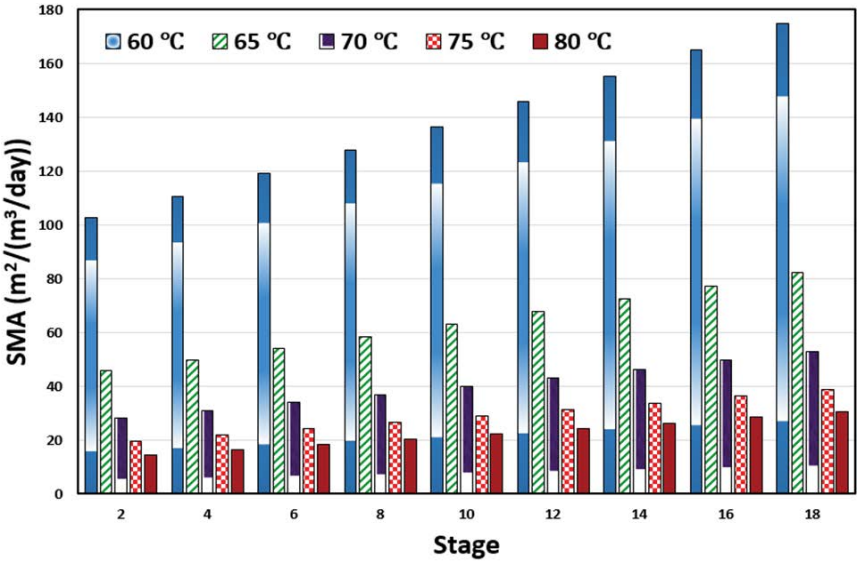

Fig. 16. Effect produced by installation of additional stages on cumulative SMA.

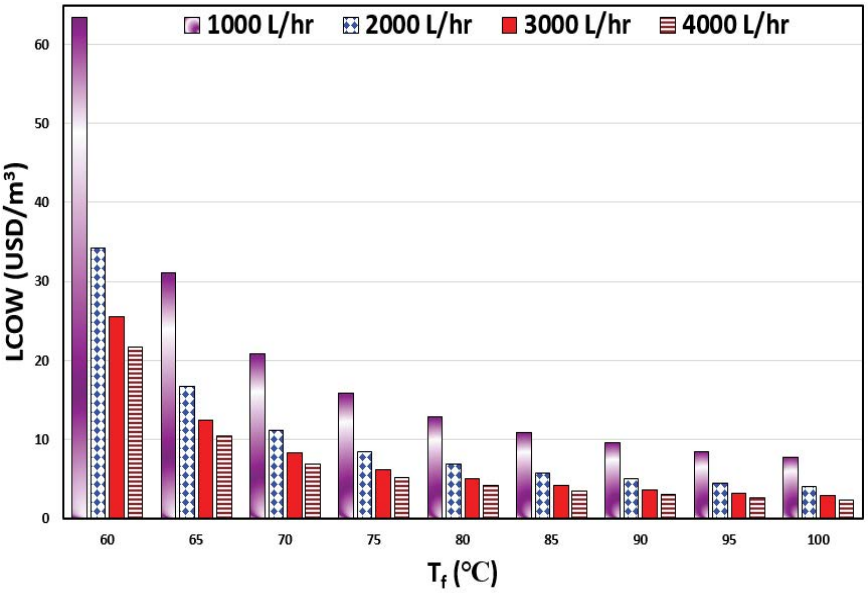

Fig. 17. Impact of feed inlet temperature on cumulative LCOW for a range of feed flowrates variating from 1,000 to 4,000 L/h.

being a denominator term tends to decrease the LCOW. Further, it can also be noted that the decrease in LCOW with the feed flowrate is more prominent when the feed flowrate is increased initially, however it continuously diminishes at higher feed flowrates.

8.4.3. Permeate side pressure

The permeate side pressure directly affects the driving force of VMD mechanism. A small change in the permeate pressure is responsible for an enormous rise or fall in the performance of VMD. Hence, it is very important to investigate the influence of permeate side pressure on the cost. Fig. 19 shows the effect of permeate side pressure on the LCOW of an 18-stage MSVMD setup, for a range of feed solution inlet temperatures varying from 60°C to 85°C. The feed flowrate and concentration were kept constant at 4,000 L/h and 0.31 gm/L.

The graph indicates that, higher permeate pressures in an MSVMD setup require more cost to produce a permeate output of 1 m^3. At a feed solution inlet temperature of 60°C, the LCOW surges from 7.139 USD/m^3 at a permeate pressure of 8 kPa to 49.45 USD/m^3 at a permeate pressure of 18 kPa. The reason for this direct relation between LCOW and the permeate side pressure is quite evident. A higher permeate pressure means lower vapor pressure (VP) difference between the saline feed side and the fresh permeate sides, resulting in a smaller flux driving potential

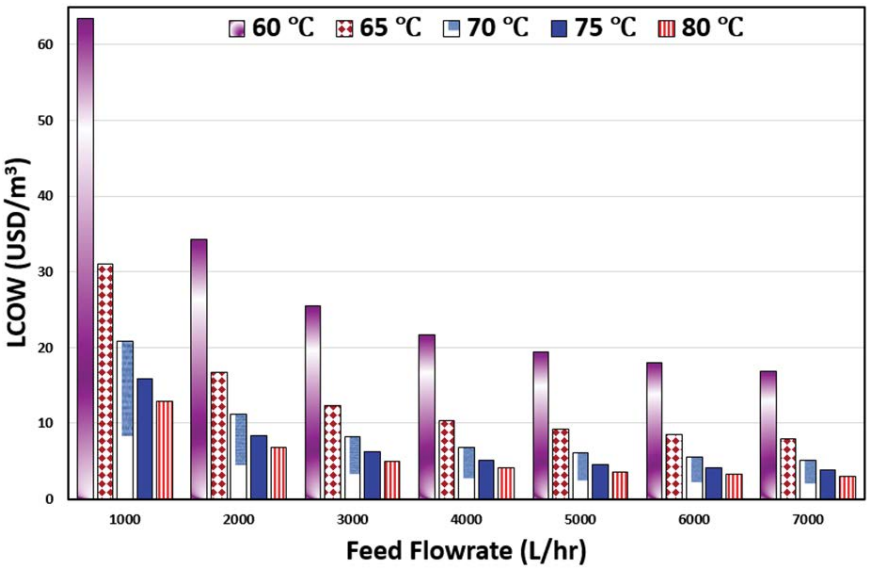

Fig. 18. Impact of feed flowrate on cumulative LCOW for feed solution inlet temperatures variating from 60°C to 80°C.

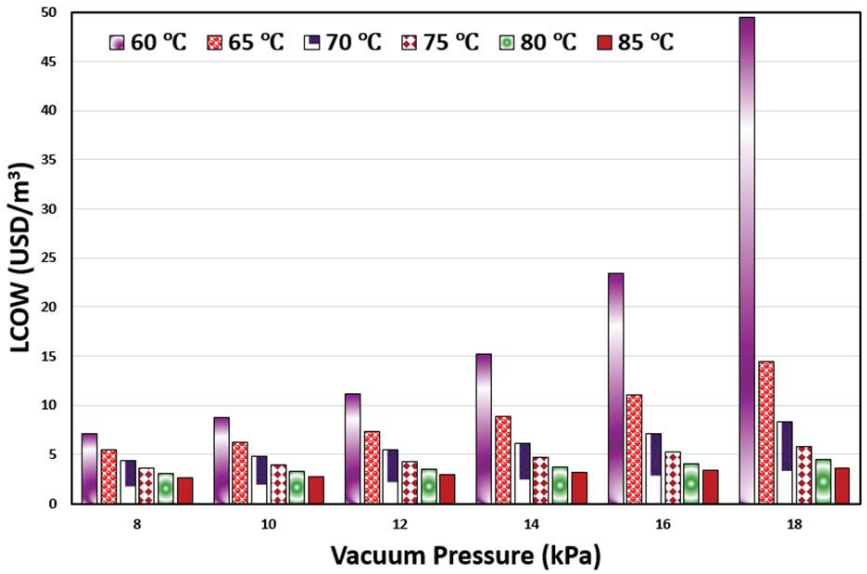

Fig. 19: Impact of permeate side pressure on cumulative LCOW for feed solution inlet temperatures variating from 60°C to 85°C.

and thus, a lower permeate output ($\dot{m}_p$), eventually causing the LCOW to rise. Similarly, the lower the permeate side pressure, the higher the VP gradient between the saline feed side and the fresh permeate sides, resulting in an enhanced permeate output ($\dot{m}_p$) from the MSVMD setup, which in turn causes a decrease in the LCOW.

8.5. Effect of multi-staging on MSVMD economics

Up till now, it is found that increasing the number of stages in an MSVMD setup improves the performance in terms of permeate output, SHC or the gained output ratio (GOR). Logically, this means that an infinite number of stages will yield the best performance, which obviously is not possible practically. Further, the cost associated with the additional number of stages must also be taken into consideration. The following section is focused to investigate the LCOW as a function of the number of stages in an MSVMD setup.

Fig. 20 shows the LCOW plotted against the number of stages in an MSVMD setup for saline feed inlet temperatures varying from 65°C to 80°C. The number of stages in the setup was varied between 2 and 18, while keeping the feed flowrate, concentration and the permeate side pressure constant at 4,000 L/h, 0.31 gm/L and 16 kPa, respectively.

It can be seen from the graph that the LCOW continued to drop down as the number of stages are increased. For example, the LCOW dropped from 80.3 USD/m^3 to

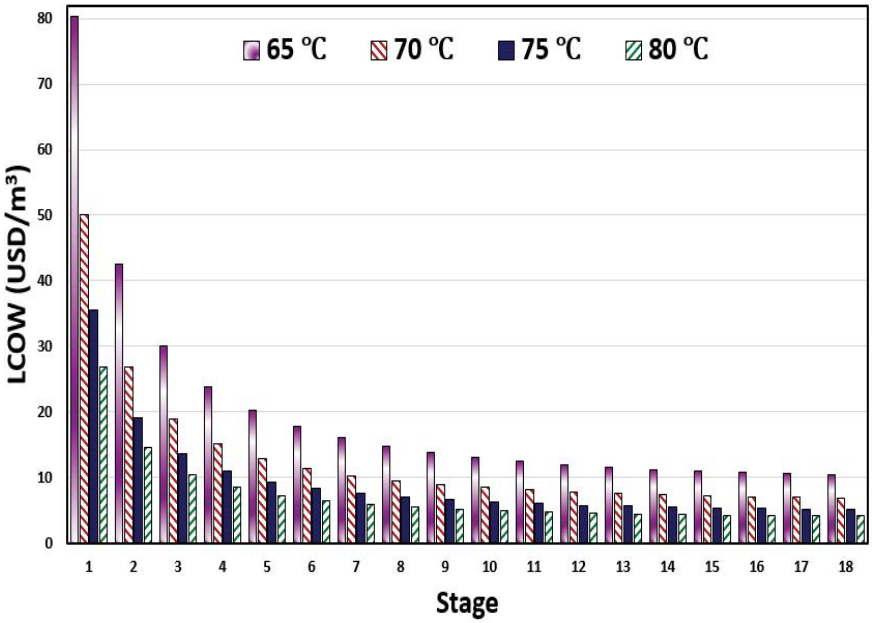

Fig. 20. Impact produced on cumulative LCOW by installation of additional stages to MSVMD.

42.59 USD/m^3 and then dropped further to 30.0 USD/m^3 as the number of stages is enhanced from 1 to 2 and then to 3, respectively, for a feed solution inlet temperature of 65°C. This dropping trend in the LCOW is obvious, as we know that increasing the number of stages enhances the permeate productivity ($\dot{m}_p$) of the MSVMD setup. But this dropping trend is more evident in initial stages and becomes trivial as the number of stages are further increased. For instance, the decrease in LCOW is 50.22 USD/m^3 when the number of stages is increased from 1 to 3, however, for the same increase in number of stages from 16 to 18 the LCOW is dropped to 0.34 USD/m^3. This is mainly due to the reason that every successive stage has a lower flux as compared to its predecessor, although the membrane area is same for both the stages (causing the same cost). Hence, it can be conveniently said that although the addition of stages drops the LCOW initially, however, a certain stage will come after which addition of any further stage will inflict a higher overall cost (Z_{eqp}, Z_{main}, Z_{inst}, brine disposal and chemical treatment cost) as compared to the rise in permeate output ($\dot{m}_p$), eventually resulting in increase in the cumulative levelized cost of water (LCOW).

It can be concluded that for a multi-stage VMD system with 18 stages, a feed inlet flowrate of 4,000 L/h and a vacuum pressure of 16 kPa, a total of 10 stages are feasible. The increase in permeate productivity of system is quite trivial with further addition of stages.

9. Conclusions

In this study, a parametric analysis of MSVMD economics was carried out in terms of SHC, GOR, and SMA. The economics of MSVMD were also analyzed based on different process variables. Finally, the impact of multi-staging on MSVMD energetics and economics was also investigated.

The key results can be summarized as follows:

- The cumulative SHC and SMA of MSVMD is lower at higher feed temperatures which is a positive aspect, however, it also induces a negative effect by reducing the GOR.
- Installation of additional stages to an MSVMD improves the performance by decreasing the SHC and raising the GOR, however, there is an upsurge in the specific membrane area (SMA) too.
- At higher feed flowrates, the cumulative SHC and GOR of MSVMD are high, whereas SMA is lower. The increase in cumulative GOR and the corresponding decrease in SMA is more prominent at lower flowrates, whereas the upsurge in SHC is more visible at higher feed flowrates.
- Additional stages in MSVMD ebbtides the cumulative SHC, however, it causes an upsurge in the GOR and SMA of the system. The SHC ebbtide and the corresponding surge in GOR is more evident at higher flowrates, whereas the increase in SMA with additional stages is independent of feed flowrate.
- The specific primary energy of system is based on the total amount of thermal energy that enters the plant (in the form of electrical energy) per m^3 of the permeate production. Since, the total heat injected into the system is always higher as compared to the energy drawn from the module, thus the specific primary energy is always going to be higher than SHC. The exergetic efficiency of the system acts as the defining parameter which differentiates between the SHC and specific primary energy consumption.
- A comparison of the SHC and GOR values indicate that SHC values are higher (when compared to literature), whereas, GOR of the system is attractive. This is due

to the reason that SHC values are determined at very high feed flowrates, that is, 1,000 to 4,000 L/h. Whereas, in literature, flowrates of 10–50 L/min are observed.
- LCOW reduces with the rise in feed inlet temperature. This reduction in LCOW is more eminent at lower feed temperatures.
- Similarly, a rising feed flowrate causes a fall in the LCOW. This behavior is more visible at low flowrates.
- LCOW has a direct relation with the permeate side pressure. The rising trend of LCOW with permeate pressure is more recognizable at higher permeate pressures.
- Having additional number of stages in an MSVMD setup brings down the cost of producing fresh water in terms of LCOW. But this trend is only for a certain number of stages, after which further addition of stages will raise the LCOW.

The present study is a comprehensive guideline for the impact of various process variables on the energetic and economic performance of MSVMD. Further, this investigation was also carried out for the impact of multi-staging on MSVMD performance. Although, the GOR is considerably improved and similarly the SHC is much reduced for MSVMD as compared to single stage VMD, but the utilization of solar energy to heat the saline feed solution through heat exchangers, might result in even higher GOR while decreasing the collective SHC.

Acknowledgements

The authors would like to thank the Higher Education Commission (HEC), Government of Pakistan for the financial support in the form of NRPU # 5550 and Ghulam Ishaq Khan Institute of Engineering Sciences and Technology for providing support during the preparation of this work.

References

[1] M. Mehanna, T. Saito, J. Yan, M. Hickner, X. Cao, X. Huang, B.E. Logan, Using microbial desalination cells to reduce water salinity prior to reverse osmosis, Energy Environ. Sci., 3 (2010) 1114–1120.
[2] A. Bajpayee, T. Luo, A. Muto, G. Chen, Very low temperature membrane-free desalination by directional solvent extraction, Energy Environ. Sci., 4 (2011) 1672–1675.
[3] A.R. Hoffman, Water security: a growing crisis and the link to energy, AIP Conf. Proc., 1044 (2008) 55–66, doi: 10.1063/1.2993738.
[4] Y. Li, K. Tian, Application of vacuum membrane distillation in water treatment, J. Sustainable Dev., 2 (2009) 183–186.
[5] S. Simone, A. Figoli, A. Criscuoli, M.C. Carnevale, A. Rosselli, E. Drioli, Preparation of hollow fibre membranes from PVDF/PVP blends and their application in VMD, J. Membr. Sci., 364 (2010) 219–232.
[6] B.R. Bodell, Distillation of Saline Water Using Silicone Rubber Membrane, United States Patents, 1968, pp. 1–4.
[7] T. Mohammadi, M. Akbarabadi, Separation of ethylene glycol solution by vacuum membrane distillation (VMD), Desalination, 181 (2005) 35–41.
[8] M.E. Findley, Vaporization through porous membranes, Ind. Eng. Chem. Process Des. Dev., 6 (1967) 226–230.
[9] C. Cabassud, D. Wirth, Membrane distillation for water desalination: how to chose an appropriate membrane?, Desalination, 157 (2003) 307–314.
[10] H. Maab, L. Francis, A.A. Saadi, C. Aubry, N. Ghaffour, G. Amy, S.P. Nunes, Synthesis and fabrication of nanostructured hydrophobic polyazole membranes for low-energy water recovery, J. Membr. Sci., 423–424 (2012) 11–19.
[11] S. Adham, A. Hussain, J.M. Matar, R. Dores, A. Janson, Application of membrane distillation for desalting brines from thermal desalination plants, Desalination, 314 (2013) 101–108.
[12] S.A. Obaidani, E. Curcio, F. Macedonio, G.D. Profio, H.A. Hinai, E. Drioli, Potential of membrane distillation in seawater desalination: thermal efficiency, sensitivity study and cost estimation, J. Membr. Sci., 323 (2008) 85–98.
[13] L.H. Cheng, Y.H. Lin, J. Chen, Enhanced air gap membrane desalination by novel finned tubular membrane modules, J. Membr. Sci., 378 (2011) 398–406.
[14] M.K. Souhaimi, T. Matsuura, Membrane Distillation, Elsevier, The Boulevard, Langford, Kidlington, Oxford, UK, 2011.
[15] M. Sudoh, K. Takuwa, H. Iizuka, K. Nagamatsuya, Effects of thermal and concentration boundary layers on vapor permeation in membrane distillation of aqueous lithium bromide solution, J. Membr. Sci., 131 (1997) 1–7.
[16] L. Martínez, F.J.F. Díaz, A. Hernández, P. Prádanos, Characterisation of three hydrophobic porous membranes used in membrane distillation: modelling and evaluation of their water vapour permeabilities, J. Membr. Sci., 203 (2002) 15–27.
[17] H.D. Baehr, K. Stephan, Heat conduction and mass diffusion, Heat and Mass Transfer, Springer, Berlin, Heidelberg 1998, pp. 105–250.
[18] M. Gryta, M. Tomaszewska, Heat transport in the membrane distillation process, J. Membr. Sci., 144 (1998) 211–222.
[19] H.C. Duong, P. Cooper, B. Nelemans, T.Y. Cath, L.D. Nghiem, Evaluating energy consumption of air gap membrane distillation for seawater desalination at pilot scale level, Sep. Purif. Technol., 166 (2016) 55–62.
[20] J. Phattaranawik, R. Jiraratananon, A.G. Fane, Heat transport and membrane distillation coefficients in direct contact membrane distillation, J. Membr. Sci., 212 (2003) 177–193.
[21] K.W. Lawson, D.R. Lloyd, Membrane distillation. I. Module design and performance evaluation using vacuum membrane distillation, J. Membr. Sci., 120 (1996) 111–121.
[22] G. Zuo, R. Wang, R. Field, A.G. Fane, Energy efficiency evaluation and economic analyses of direct contact membrane distillation system using Aspen Plus, Desalination, 283 (2011) 237–244.
[23] G. Chen, X. Yang, R. Wang, A.G. Fane, Performance enhancement and scaling control with gas bubbling in direct contact membrane distillation, Desalination, 308 (2013) 47–55.
[24] M.A.I. Gil, G. Jonsson, Factors affecting flux and ethanol separation performance in vacuum membrane distillation (VMD), J. Membr. Sci., 214 (2003) 113–130.
[25] H. Zhao, H. Sun, Study on the experiment of concentrating coking wastewaters by air-blowing vacuum membrane distillation, Appl. Phys. Res., 1 (2009) 53–58.
[26] D. Wirth, C. Cabassud, Water desalination using membrane distillation: comparison between inside/out and outside/in permeation, Desalination, 147 (2002) 139–145.
[27] T. Mohammadi, M.A. Safavi, Application of Taguchi method in optimization of desalination by vacuum membrane distillation, Desalination, 249 (2009) 83–89.
[28] Z. Si, D. Han, J. Gu, J. Chen, M. Zheng, Y. Song, N. Mao, Study on vacuum membrane distillation coupled with mechanical vapor recompression system for the concentration of sulfuric acid solution, J. Braz. Soc. Mech. Sci. Eng., 41 (2019) 1–15.
[29] Y.D. Kim, W.S. Kim, Experimental and Theoretical Investigations of a Novel Multi-Stage Direct Contact Membrane Distillation Module, Proceedings of the 2nd World Congress on New Technologies, NEWTECH 2016 – Budapest, Hungary, 2016.
[30] A. Omar, A. Nashed, R. Taylor, Single vs Multi-Stage Vacuum Membrane Distillation: An Energetic Analysis, Proceedings of the 11th Australasian Heat and Mass Transfer Conference, AHMTC11, RMIT University, Melbourne, Australia, 2018, p. 11.
[31] N. Ghaffour, S. Soukane, J.G. Lee, Y. Kim, A. Alpatova, Membrane distillation hybrids for water production and energy efficiency enhancement: a critical review, Appl. Energy, 254 (2019) 113698, doi: 10.1016/j.apenergy.2019.113698.

[32] J. Gilron, L. Song, K.K. Sirkar, Design for cascade of crossflow direct contact membrane distillation, Ind. Eng. Chem. Res., 46 (2007) 2324–2334.
[33] F. He, J. Gilron, K.K. Sirkar, High water recovery in direct contact membrane distillation using a series of cascades, Desalination, 323 (2013) 48–54.
[34] Y. Lu, J. Chen, Optimal design of multistage membrane distillation systems for water purification, Ind. Eng. Chem. Res., 50 (2011) 7345–7354.
[35] S.M. Shim, J.G. Lee, W.S. Kim, Performance simulation of a multi-VMD desalination process including the recycle flow, Desalination, 338 (2014) 39–48.
[36] E.K. Summers, J.H. Lienhard V, Cycle Performance of Multi-Stage Vacuum Membrane Distillation (Ms-Vmd) Systems, The International Desalination Association World Congress on Desalination and Water Reuse 2013, Tianjin, China, 2013.
[37] H.W. Chung, J. Swaminathan, D.M. Warsinger, J.H. Lienhard V, Multistage vacuum membrane distillation (MSVMD) systems for high salinity applications, J. Membr. Sci., 497 (2016) 128–141.
[38] K. Zhao, W. Heinzl, M. Wenzel, S. Büttner, F. Bollen, G. Lange, S. Heinzl, N. Sarda, Experimental study of the memsys vacuum-multi-effect-membrane-distillation (V-MEMD) module, Desalination, 323 (2013) 150–160.
[39] E. Jang, S.H. Nam, T.M. Hwang, S. Lee, Y. Choi, Effect of operating parameters on temperature and concentration polarization in vacuum membrane distillation process, Desal. Water Treat., 54 (2015) 871–880.
[40] F.H. Choo, M.K. Ja, K. Zhao, A. Chakraborty, E.T.M. Dass, M. Prabu, B. Li, S. Dubey, Experimental study on the performance of membrane based multieffect dehumidifier regenerator powered by solar energy, Energy Procedia, 48 (2014) 535–542.
[41] P. Boutikos, E.S. Mohamed, E. Mathioulakis, V. Belessiotis, A theoretical approach of a vacuum multi-effect membrane distillation system, Desalination, 422 (2017) 25–41.
[42] R. Lefers, N.M.S. Bettahalli, N. Fedoroff, S.P. Nunes, T.O. Leiknes, Vacuum membrane distillation of liquid desiccants utilizing hollow fiber membranes, Sep. Purif. Technol., 199 (2018) 57–63.
[43] N. Hoda, S.V. Suggala, P.K. Bhattacharya, Pervaporation of hydrazine-water through hollow fiber module: modeling and simulation, Comput. Chem. Eng., 30 (2005) 202–214.
[44] L.H. Cheng, P.C. Wu, J. Chen, Modeling and optimization of hollow fiber DCMD module for desalination, J. Membr. Sci., 318 (2008) 154–166.
[45] G. Ramon, Y. Agnon, C. Dosoretz, Heat transfer in vacuum membrane distillation: effect of velocity slip, J. Membr. Sci., 331 (2009) 117–125.
[46] H.G. Grohn, Influence of the Yaw Angle on Heat Transfer and Pressure Drop of Helical Type Heat Exchangers, International Atomic Energy Agency, IAEA, Vienna, Austria, 1988.
[47] J. Liu, C. Wu, X. Lü, Heat and mass transfer in vacuum membrane distillation, Huagong Xuebao/CIESC J., 62 (2011) 908–915.
[48] R.W. Schofield, A.G. Fane, C.J.D. Fell, Heat and mass transfer in membrane distillation, J. Membr. Sci., 33 (1987) 299–313.
[49] A.S. Alsaadi, N. Ghaffour, J.D. Li, S. Gray, L. Francis, H. Maab, G.L. Amy, Modeling of air-gap membrane distillation process: a theoretical and experimental study, J. Membr. Sci., 445 (2013) 53–65.
[50] M.I. Soomro, W.S. Kim, Parabolic-trough plant integrated with direct-contact membrane distillation system: concept, simulation, performance, and economic evaluation, Sol. Energy, 173 (2018) 348–361.
[51] M.R. Elmarghany, A.H. El-Shazly, M.S. Salem, M.N. Sabry, N. Nady, Thermal analysis evaluation of direct contact membrane distillation system, Case Stud. Therm. Eng., 13 (2019) 100377, doi: 10.1016/j.csite.2018.100377.
[52] M. Khayet, Solar desalination by membrane distillation: dispersion in energy consumption analysis and water production costs (a review), Desalination, 308 (2013) 89–101.
[53] M.S. Peters, J.I. Peters, Plant Design and Economics for Chemical Engineers, McGraw-Hill, New York, 1959, pp. 27–30.
[54] K. Park, J.H. Kim, H.S. Kim, K.Y. Lee, D.R. Yang, K.N. Kim, Economic analysis of geothermal energy and VMD desalination hybrid process, Clean Technol., 20 (2014) 13–21.
[55] M. Kolhe, S. Kolhe, J.C. Joshi, Economic viability of stand-alone solar photovoltaic system in comparison with diesel-powered system for India, Energy Econ., 24 (2002) 155–165.
[56] A. Nashed, High Recovery Rate Solar Driven Reverse Osmosis and Membrane Distillation Plants for Brackish Groundwater Desalination in Egypt, Ph.D. Dissertation, University of New South Wales Sydney, Australia, 2014.